Nature of field-induced antiferromagnetic order in Zn-doped CeCoIn$_5$ and its connection to quantum criticality in the pure compound

Makoto Yokoyama ⬤,* Yutoku Honma, Yoshiki Oshima, Rahmanto, and Kohei Suzuki
Faculty of Science, Ibaraki University, Mito, Ibaraki 310-8512, Japan
and Institute of Quantum Beam Science, Ibaraki University, Mito, Ibaraki 310-8512, Japan

Kenichi Tenya
Faculty of Education, Shinshu University, Nagano 380-8544, Japan

Yusei Shimizu and Dai Aoki
Institute for Materials Research, Tohoku University, Oarai, Ibaraki 311-1313, Japan

Akira Matsuo, Koichi Kindo, Shota Nakamura,† Yohei Kono,‡ Shunichiro Kittaka,‡ and Toshiro Sakakibara
Institute for Solid State Physics, The University of Tokyo, Kashiwa, Chiba 277-8581, Japan

Quantum criticality plays an important role in the unconventional nature of superconductivity in strongly correlated electron systems. However, the intrinsic antiferromagnetic (AFM) order parameter responsible for quantum criticality has been unidentified in the prototypical unconventional superconductor CeCoIn$_5$. In this work, magnetization and specific-heat measurements for CeCo(In$_{1-x}$Zn$_x$)$_5$ with $x \leqslant 0.07$ demonstrate that the field-induced AFM order develops with Zn doping, along with a continuous increase in its critical field up to 10 T at $x = 0.07$. The weak signals associated with the AFM phase transition strongly suggest spatially inhomogeneous evolution of the AFM phase, whose feature becomes pronounced with decreasing the Zn concentration. The temperature, magnetic field, and Zn concentration phase diagram is constructed from those experimental results. It is found that, in this diagram, extrapolating the x dependence of the AFM critical field yields the value of ≈ 5 T for $x \to 0$, which coincides with the location of the quantum critical point in CeCoIn$_5$. The specific heat shows $-\ln T$ diverging behavior characteristic of the non-Fermi-liquid state at the AFM critical fields for all of the x range. The scaling analysis for the specific-heat data above critical fields leads to continuous variations of the scaling parameters as a function of x. These findings provide strong evidence that the quantum critical fluctuations in CeCoIn$_5$ originate from the order parameter corresponding to the field-induced AFM state observed in Zn-doped systems.

I. INTRODUCTION

In recent years, there has been growing interest in the nature of the unusual superconducting (SC) states that emerge in the vicinity of a quantum critical point (QCP) in strongly correlated electron systems [1–4]. The heavy-fermion superconductor CeCoIn$_5$ (a HoCoGa$_5$-type tetragonal structure; SC transition temperature of $T_c = 2.3$ K) is a prototypical compound showing the interplay of unusual SC properties and magnetic quantum critical fluctuations [5]. The magnetic origin of the Cooper pairing is inferred from the d-wave ($d_{x^2-y^2}$) symmetry of the SC gap [6–8]. Couplings between the antiferromagnetic (AFM) spin correlations and the SC order are further suggested from the observations of a spin-resonance excitation in the SC phase [9–17] and an alternative SC phase that coexists with an incommensurate AFM spin modulation (the Q phase) just below H_{c2} under the magnetic field B along the tetragonal c plane [18–25]. At the same time, this compound shows non-Fermi-liquid (NFL) behavior in the paramagnetic region above $\mu_0 H_{c2} = 5$ T for $B \parallel c$, such as a $-\ln T$ divergence in specific heat divided by temperature C/T, T-linear behavior in electrical resistivity and magnetization, and a strong enhancement of the nuclear spin-lattice relaxation rate [26–30]. It is believed that the development of AFM quantum critical fluctuations causes this NFL behavior and leads to the anomalous SC properties in CeCoIn$_5$. However, the origin of the quantum critical fluctuations has not been clarified because an obvious AFM order relevant to the quantum critical fluctuations is absent in this compound.

Many researchers have searched for the AFM phases intensively using ionic substitution techniques, as well as an extremely-low-temperature experiment for CeCoIn$_5$ [31]. It has been revealed that the substitutions of Nd and Sm for

---

*makoto.yokoyama.sci@vc.ibaraki.ac.jp

†Present address: Department of Physical Science and Engineering, Nagoya Institute of Technology, Nagoya 466-8555, Japan.

‡Present address: Department of Physics, Chuo University, Kasuga, Bunkyo-ku, Tokyo 112-8551, Japan.

Ce [32–35], Rh for Co [36–40], and Cd, Hg, and Zn for In [41–46] can induce long-range AFM order. Substituting Rh for Co induces the commensurate AFM order and the incommensurate spiral orders with the spins polarized along the c plane [36–40]. The AFM phase with the same commensurate spin modulation also emerges in the Cd- and Hg-doped alloys, but the AFM-ordered moments are considered to be polarized along the c axis [13,41–44]. Moreover, Nd-doped CeCoIn$_5$ exhibits two incommensurate AFM orders (the spin-density wave phase and the Q phase) that coexist with the superconducting state [32–34]. These findings strongly suggest that the multiple AFM correlations are hidden in CeCoIn$_5$, but it is unclear what kind of the AFM correlation governs the quantum critical phenomena and significantly affects the unconventional SC properties.

In the mixed compound CeCo(In$_{1-x}$Zn$_x$)$_5$, the doping of Zn suppresses the SC transition temperature T_c from 2.3 K ($x = 0$) to 1.3 K ($x = 0.07$); then the AFM order (the low-field AFM phase) emerges below $T_N = 2.2$ K for $x \geqslant 0.05$ [45,46]. For $x = 0.07$, in addition, applying B along the c axis generates the other AFM order (the high-field AFM phase) in the B range of 5–10 T, whose order parameter is clearly distinguished from the low-field AFM phase located below $B_{M1} = 5$ T and the SC phase below $\mu_0 H_{c2} = 3$ T [47]. The nuclear magnetic resonance measurement reveals that the low-field and high-field AFM orders have commensurate and incommensurate spin structures, respectively [48]. Clear $C/T \propto -\ln T$ behavior occurs at the upper critical field of the high-field AFM phase ($B_{M2} \simeq 10$ T), indicating the presence of the QCP of the high-field AFM phase at B_{M2} and $T = 0$ [47]. Furthermore, it has been found that, for pure and Zn 7%-doped CeCoIn$_5$, the C/T data above the critical field B_0 (5 T for $x = 0$ and 10 T for $x = 0.07$) are well scaled by the nearly identical logarithmic function of B and T: $\ln[(B - B_0)/T^\beta]$ with $\beta \approx 2.7$ [26,47]. This similarity in the C/T data between the two compounds suggests that field-induced quantum critical fluctuations have almost the same origin. However, it is unclear how the high-field AFM order parameter contributes to the quantum critical fluctuations in CeCoIn$_5$ because the nature of the high-field AFM phase and its quantum critical fluctuations is unknown in the intermediate Zn concentrations between $x = 0$ and 0.07. For instance, it was reported that the AFM order was not detected by a scanning tunneling microprobe in the very small Zn concentration range for $x \leqslant 0.007$ in epitaxial films of Zn-doped CeCoIn$_5$ [49].

It is important to find the AFM mode responsible for the quantum criticality among the existing AFM correlations in CeCoIn$_5$, because this information would be indispensable for comprehensively understanding the origins of the quantum criticality and the unconventional SC properties. Among the ionic substitutions of CeCoIn$_5$, CeCo(In$_{1-x}$Zn$_x$)$_5$ is a unique doped system exhibiting antiferromagnetism and its concomitant field-induced quantum criticality [47]. Therefore, it is crucial to clarify the connection between the quantum criticality in pure CeCoIn$_5$ [26,27] and the high-field AFM order in the Zn 7%-doped alloy [47]. To trace the origin of quantum criticality, we comprehensively investigated the high-field AFM state and NFL behavior in CeCo(In$_{1-x}$Zn$_x$)$_5$ for $x \leqslant 0.07$ by performing magnetization and specific-heat measurements with a c-axis magnetic field. In this paper,

we demonstrate that the high-field AFM order continuously shrinks and becomes weak along with the suppression of its critical field as the doped Zn amount is decreased from 7% to 0%, while the $C/T \propto -\ln T$ behavior at the critical field, characteristic of quantum criticality, is unchanged. The weak signals associated with the high-field AFM transition in magnetization and specific heat strongly suggest spatially inhomogeneous evolution of the AFM phase, whose feature becomes pronounced with decreasing Zn concentration. The precise phase diagram concerning temperature, c-axis magnetic field, and Zn concentration is constructed for CeCo(In$_{1-x}$Zn$_x$)$_5$. In addition, a scaling analysis for the C/T data above the critical fields yields nearly the same β values in the variable $\ln[(B - B_0)/T^\beta]$ involved in the scaling function for the entire Zn concentration range investigated. The spin correlations concerning the high-field AFM state are considered to underlie all of these features. In particular, we confirm that the field-induced quantum critical fluctuations in pure CeCoIn$_5$ come from the instability of the hidden AFM order parameter, which emerges as the high-field AFM order in the Zn-doped alloys, as suggested previously [47].

II. EXPERIMENT DETAILS

Single crystals of CeCo(In$_{1-x}$Zn$_x$)$_5$ with $x = 0$, 0.025, 0.035, 0.05, and 0.07 were grown with an indium-flux method, whose details have been previously described [45,46]. Note that the actual Zn concentration y, estimated using an energy dispersive x-ray spectroscopy (EDS) technique, is roughly 35% of the nominal (starting) concentration x for the sample with each x, although it involves the fairly large uncertainty unavoidable in EDS measurements [46]. Therefore, for clarity and simplicity we use the nominal concentration x throughout this paper. The c-axis magnetization M was measured in temperatures as low as 0.08 K with a capacitively detected Faraday force magnetometer [50]. The specific heat C measurement was performed down to 0.5 K with the thermal relaxation method using a commercial measurement system (PPMS, Quantum Design). In both measurements, external magnetic field B ($\mu_0 H$) was applied up to 14 T along the c axis.

III. RESULTS

A. Emergence of the field-induced antiferromagnetic state in Zn-doped CeCoIn$_5$

Displayed in Figs. 1(a)–1(d) are the field variations of c-axis magnetization $M(B)$ at 0.08 K for $x = 0.025$, 0.035, 0.05, and 0.07, respectively. The SC upper critical field $\mu_0 H_{c2}$ is estimated to be ≈ 5 T for $x \leqslant 0.05$ and 3 T for $x = 0.07$ from the closing of the hysteresis in the $M(B)$ curves measured under increasing and decreasing field variations. The first-order nature of the SC pair breaking at H_{c2} is confirmed by the discontinuous jump in $M(B)$ at $x = 0.025$, but this feature is smeared due to the large hysteresis and the peak effect in $M(B)$ for $x \geqslant 0.05$. These observations are consistent with previous $M(B)$ measurements at 0.27 K [46].

We focus on the $M(B)$ curves above $\mu_0 H_{c2}$ to derive the nature of the magnetic states in CeCo(In$_{1-x}$Zn$_x$)$_5$. At $x = 0.07$, $M(B)$ exhibits a step-like increase at $B_{M1} = 5.0(5)$ T and a
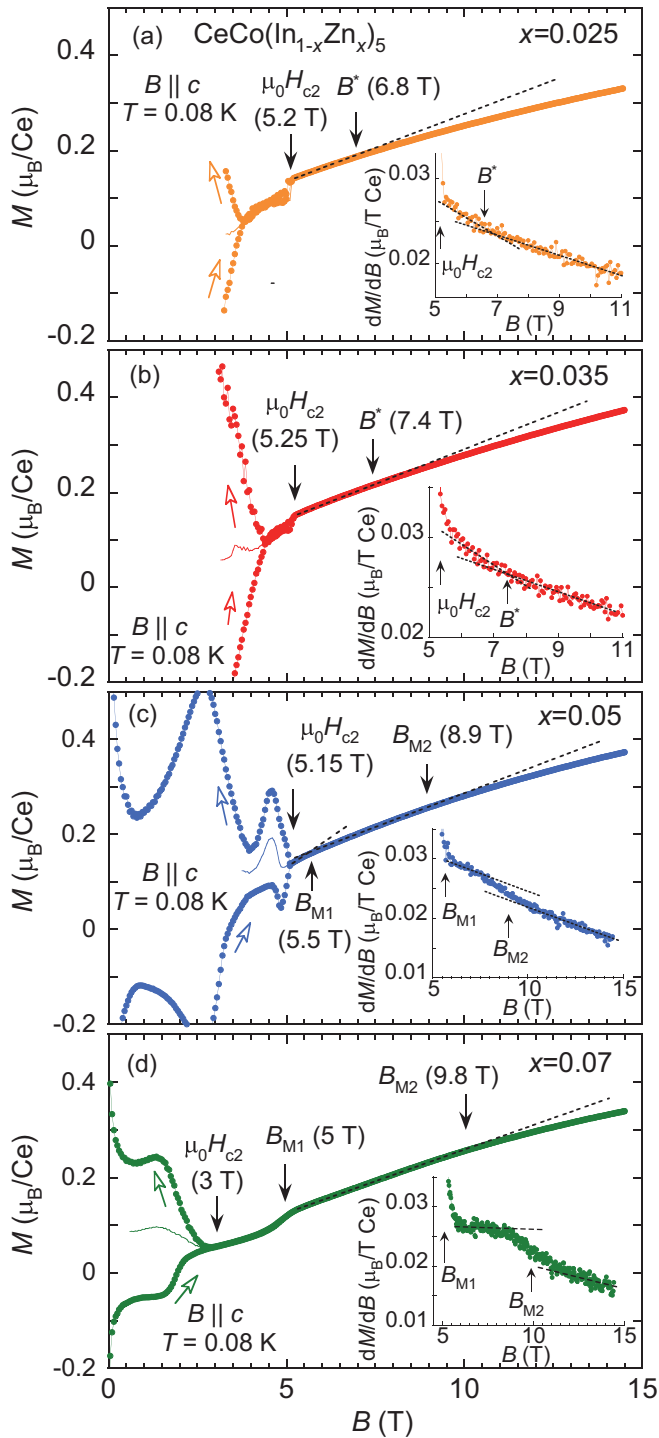
FIG. 1. Magnetic-field dependence of c-axis magnetization M at 0.08 K for CeCo(In$_{1-x}$Zn$_x$)$_5$ with (a) $x = 0.025$, (b) 0.035, (c) 0.05, and (d) 0.07 [47]. The open arrows indicate the directions of the B sweep, and the solid curves for $B < \mu_0 H_{c2}$ are the average of the magnetization between the increasing and decreasing field variations. The insets show the dM/dB plot above 5 T. The dashed lines are guides for the eye.

weak kink or bending at $B_{M2} = 9.8(6)$ T [Fig. 1(d)] [47]. The former originates from the phase transition between the low-field AFM order and the high-field AFM order, and the latter corresponds to the critical field of the high-field

AFM phase [47]. For $x = 0.05$, a very weak kink occurs at $B_{M1} = 5.5(2)$ T in $M(B)$ instead of the step-like anomaly [Fig. 1(c) and its inset] as we reported previously [45], which may appear as a part of the step-like change because the condition of $\mu_0 H_{c2} \approx B_{M1}$ is realized in this x range [51]. The present investigation further reveals a weak kink or bending feature at $B_{M2} = 8.9(8)$ T in $M(B)$ for $x = 0.05$, along with a reduction of B_{M2} from the value for $x = 0.07$. The weak kink or bending feature at B_{M2} in $M(B)$ can be confirmed by the step-like variation in dM/dB for $x = 0.05$ and 0.07 [the insets in Figs. 1(c) and 1(d)]. The anomaly at B_{M2} in $M(B)$ becomes obscure for the lower Zn concentrations of $x = 0.025$ and 0.035 [Figs. 1(a) and 1(b)], but dM/dB shows a bending at $B^* \approx 6.8$ T and ≈ 7.4 T, respectively [the insets in Figs. 1(a) and 1(b)]. Note that these B^* values are significantly larger than the first-order SC upper critical fields. These trends concerning the kink in $M(B)$ at $\approx B_{M2}$ (or B^*) suggest that the high-field AFM order (or correlation) likely occurs for $x \geqslant 0.025$, although it becomes weak and unstable along with the reduction of B_{M2} as the Zn concentration is decreased. In particular, the significant broadening of the anomaly at B_{M2} in $M(B)$ even for $x \geqslant 0.05$ would stem from heterogeneous emergence of the high-field AFM order, as will be argued later. An additional reason for the smallness of the AFM signals in magnetization would be related to the AFM structure of the high-field AFM order. The recent NMR experiment for Zn 7%-doped CoCoIn$_5$ revealed that the high-field AFM structure has an incommensurate spin modulation, and a direction of the staggered spins is perpendicular to the applied c-axis magnetic field [48]. In such a situation, the anomaly in the c-axis magnetization associated with the AFM transition could be small.

Suppression of the high-field AFM phase with decreasing x is also found in the temperature variations of the c-axis magnetization divided by the magnetic field M/B, as shown in Figs. 2(a)–2(d). For $x = 0.07$, M/B exhibits a broad peak due to the high-field AFM ordering at $T_{M2} \approx 0.8$ K and $B = 7$ T [Fig. 2(d)] [47]. T_{M2} is reduced by increasing B and approaches zero for $B \to B_{M2}$. The phase transition at T_{M2} is also confirmed by a jump in specific heat C [Fig. 2(f)] [47]. Similar trends are also seen in M/B [Fig. 2(c)] and C [Fig. 2(e)] for $x = 0.05$. The $C(T)$ curve for $B = 6$ T exhibits a jump at $T_{M2} \approx 0.58$ K. However, the jump moves out of the lowest accessible temperature range (0.5 K) for $B \geqslant 7$ T, whereas its "tail" is observed below ≈ 1 K. At the same time, the peak at T_{M2} in M/B becomes unclear for $B \geqslant 7$ T, suggesting the high-field AFM order is weakened by decreasing the Zn concentration, similar to the interpretation derived from the $M(B)$ data. For $x = 0.025$ and 0.035, no clear feature associated with the high-field AFM transition is seen in M/B [Figs. 2(a) and 2(b)] and C (not shown). Nevertheless, the temperature variations of M/B at 5.5 and 6 T for $x = 0.035$ exhibits a weak suppressing (nearly-T-constant) feature for $T \to 0$ compared with M/B for the higher B range, such as that for 8 T. Because this B range is larger than $\mu_0 H_{c2}$ [$=5.25(5)$ T], at which the breakdown of the SC order involves the nearly-first-order nature [Fig. 1(b)], we consider that the AFM correlations certainly exist at least for $x = 0.035$.
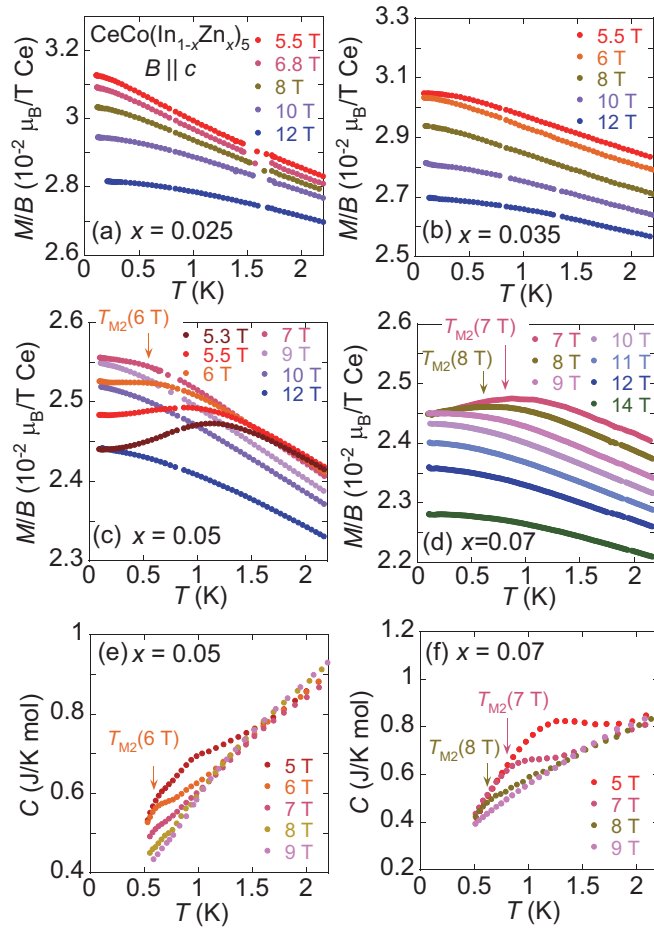
FIG. 2. Temperature variations of the *c*-axis magnetization divided by the magnetic field M/B for $CeCo(In_{1-x}Zn_x)_5$ with (a) $x = 0.025$, (b) 0.035, (c) 0.05, and (d) 0.07 [47], and the specific heat C for (e) $x = 0.05$ and (f) 0.07 [47], measured for the $B \parallel c$ condition. Note that only data for high B ranges above 5 T are shown in these plots.

In Figs. 3(a)–3(d), we display the magnetic field versus temperature (*B-T*) phase diagram for $CeCo(In_{1-x}Zn_x)_5$ with $x = 0.025$, 0.035, 0.05, and 0.07, respectively, obtained from the magnetization and specific-heat data for $B \parallel c$. The SC and low-field AFM phase boundaries have been clarified in previous studies [45–47,51]. In those plots, the exponent n of $M/B \propto -T^n$ for $B > 5$ T is also shown, which is estimated from the M/B data via a simple relation: $n = T/(M/B) \, d(M/B)/dT$. We simply assume this function because the temperature dependencies of M/B are convex upward [Figs. 2(a)–2(d)]. It is convenient to tentatively use this expression because the AFM-order state and the Fermi-liquid (FL) state can be recognized as the $n \lesssim 0$ and $n \approx 0$ regions, respectively, in the *B-T* phase diagram. The distribution of the n value well reflects the high-field AFM region below B_{M2} for $x = 0.07$ [Fig. 3(d)], which is consistent with the boundary derived from the specific-heat and magnetization data [47]. It is clearly seen in Figs. 3(a)–3(d) that the area of the high-field AFM order is reduced by decreasing the Zn concentration. For $x = 0.05$, the emergence of the high-field AFM phase is identified by the exponent n and the phase boundary [Fig. 3(c)].

However, a phase boundary of the high-field AFM order could not be estimated for $x = 0.025$ and 0.03 because no clear anomaly is detected in the specific-heat and magnetization data. Nevertheless, the observation of a small $n \approx 0$ region between $\mu_0 H_{c2}$ and B^* for $x = 0.035$, corresponding to a triangle area in the *B-T* phase diagram in Fig. 3(b), implies the existence of the high-field AFM state, although it may occur heterogeneously or as short-ranged order. These features strongly suggest that B^* ($x \leqslant 0.035$) and B_{M2} ($x \geqslant 0.05$) are regarded as the critical field of the high-field AFM state. At the same time, B^* and B_{M2} are considered to correspond to the QCP of the high-field AFM state because the Fermi-liquid ($n \approx 0$) region for $B > B^*$ and $B > B_{M2}$ tends to shrink as B is reduced toward B^* and B_{M2} [Figs. 3(a)–3(d)]. The features above concerning the high-field AFM order, NFL and FL states, and locations of the QCP are summarized in the temperature, magnetic field, and nominal Zn concentration phase diagram (Fig. 4).

B. The origin of quantum criticality in pure and Zn-doped CeCoIn₅

To clarify the nature of quantum criticality and its relation to the high-field AFM state, we next investigate the NFL behavior in the specific heat for $B \geqslant B^*$ ($x \leqslant 0.035$) and $B \geqslant B_{M2}$ ($x \geqslant 0.05$). Figures 5(a)–5(d) display the $4f$ electronic specific heat divided by the temperature C_e/T for $CeCo(In_{1-x}Zn_x)_5$ with $x = 0.025$, 0.035, 0.05, and 0.07 [47], respectively. In those plots, the C_e values were obtained by carefully subtracting the phonon and nuclear-spin contributions from the measured C data. The phonon and nuclear-spin contributions were estimated using the C data of non-$4f$ compound $LaCoIn_5$ at $B = 0$ and the calculations based on the natural abundance of nuclear spins including ^{59}Co, ^{113}In, and ^{115}In, respectively. Note that the phonon contribution in C is about 10% even at 4 K for all the Zn concentrations, and, therefore, the effect of Zn doping (actual Zn concentration: roughly 35% of x) is negligible at low temperatures. A similar situation is realized in the estimation of the nuclear-spin contribution; the ambiguity of the Zn concentrations in the samples yields an error of 3% in C_e for $T \geqslant 0.5$ K and $B \leqslant 14$ T at most. However, we do not estimate C_e below 0.5 K because the nuclear-spin contribution is expected to be very large and become more than 95% of C at 0.1 K for $B \geqslant 10$ T. In CeCoIn₅, nuclear level splitting has been observed in C below ≈ 0.1 K even at $B = 0$ [18,52]. In this paper, this effect was taken into account by simply assuming an additional effective magnetic field (≈ 1.5 T) in the estimation of the nuclear-spin contributions in C. We confirmed that this effect slightly changes the C_e values only at ≈ 0.5 K (1% at 7 T and 5% at 14 T at most), but hardly influences the scaling analysis described below.

It is found that C_e/T is roughly in proportion to the $-\ln T$ function at $\approx B^*$ and $\approx B_{M2}$ for all of the x range investigated. The magnetic field at which the $-\ln T$ behavior occurs in C_e/T is always linked with B^* and B_{M2} determined by the magnetization, indicating that the anomaly in magnetization curve is intrinsic although it is very weak [Figs. 1(a)–1(d)]. A slight deviation from the $-\ln T$ dependence occurs in C_e/T at low temperatures for $x = 0.025$ and 0.035 [Figs. 5(a)
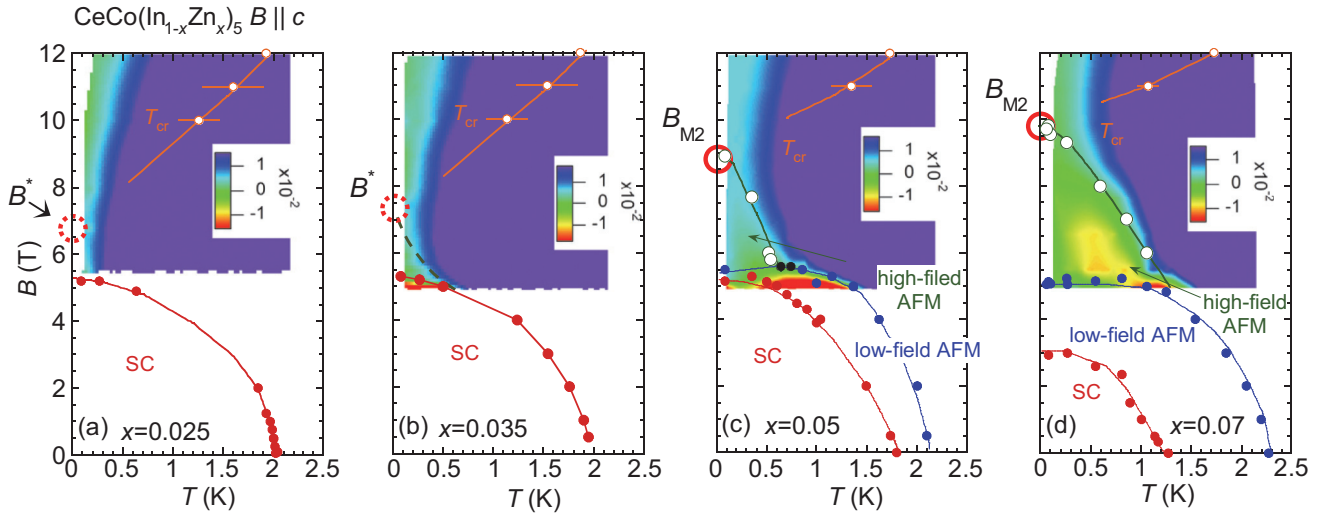
FIG. 3. The magnetic field versus temperature phase diagram for $CeCo(In_{1-x}Zn_x)_5$ with (a) $x = 0.025$, (b) 0.035, (c) 0.05, and (d) 0.07 [47] obtained from the magnetization and specific-heat measurements for $B \parallel c$. The image plots represent the exponent n estimated by assuming the relation of $M/B \propto -T^n$. The $n \lesssim 0$ and $n \approx 0$ areas suggest the AFM and Fermi-liquid regions, respectively. The red open circles represent B_{M2} or B^* estimated from the magnetization curve $M(B)$ at 0.08 K. Note that the very weak anomaly at B^* in $M(B)$ for $x = 0.025$ and 0.035 possibly originates from the heterogeneous or short-range AFM order [see Figs. 1(a) and 1(b) and their insets]. The dashed line in panel (b) indicates possible short-range AFM ordering characterized by small n values (see text).

and 5(b)], possibly caused by an effect of the blurred transition at $\approx B^*$, as observed in the $M(B)$ curves [Figs. 1(a) and 1(b) and those insets]. The $-\ln T$ diverging behavior in C_e/T gradually changes into T-constant behavior or broad peak with increasing B, reflecting a NFL-FL crossover due to the suppression of the AFM quantum critical fluctuations. The crossover temperature T_{cr}, defined as a deviation from the $-\ln T$ function in C_e/T, approaches B^* or B_{M2} for $T \to 0$
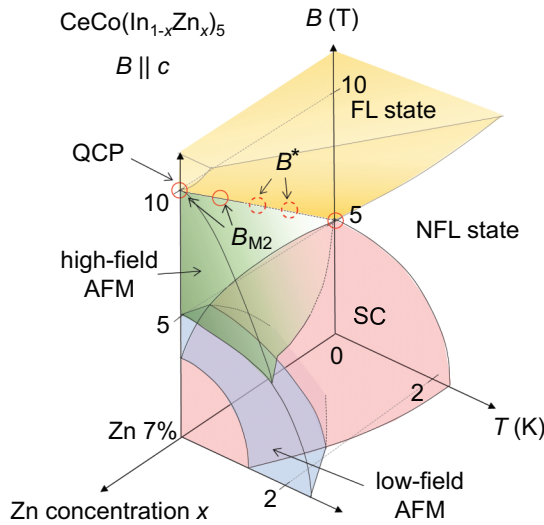

FIG. 4. A T-B-x phase diagram for $CeCo(In_{1-x}Zn_x)_5$, which is expected from the present experimental result and the previous results [27,45–47]. The red open circles represent the locations of the QCP. Note that the high-field AFM order is considered to occur heterogeneously or as short-ranged order, and the heterogeneous feature becomes pronounced with decreasing x.
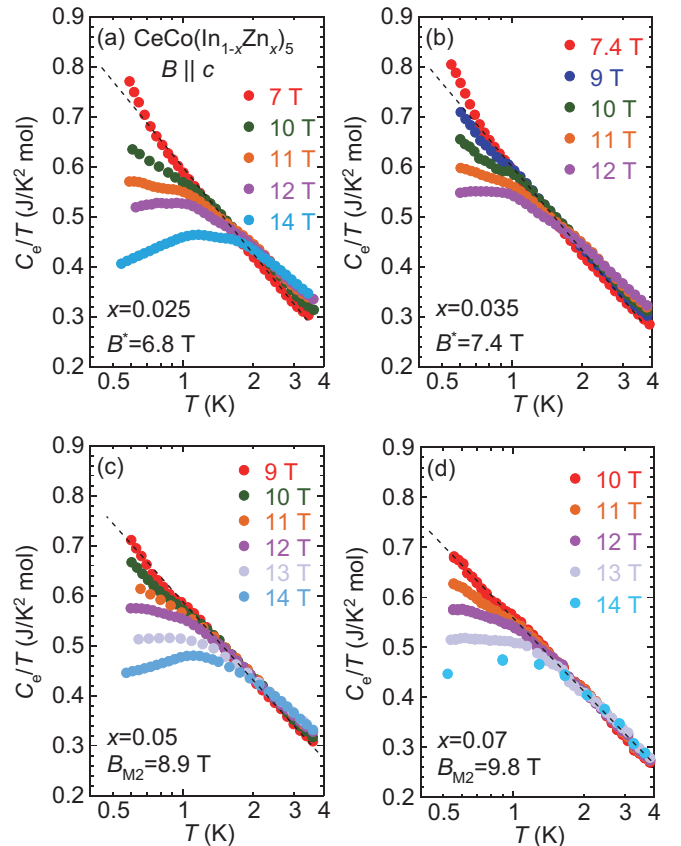

FIG. 5. Temperature variations of the $4f$ electronic specific heat divided by the temperature C_e/T for $CeCo(In_{1-x}Zn_x)_5$ with (a) $x = 0.025$, (b) 0.035, (c) 0.05, and (d) 0.07 [47], measured in the paramagnetic phase above B^* ($x \leqslant 0.035$) and B_{M2} ($x \geqslant 0.05$) for $B \parallel c$. The dashed lines indicate a guide for the $-\ln T$ function.
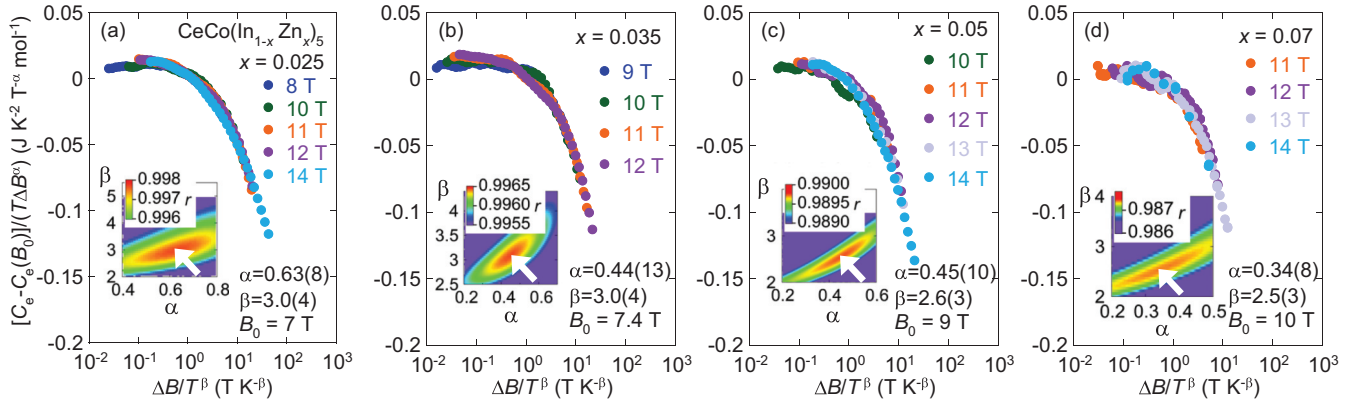
FIG. 6. The curves of $[C_e - C_e(B_0)]/(T\Delta B^\alpha)$ versus $\Delta B/T^\beta$ obtained from the scaling analysis of the C_e/T data for CeCo(In$_{1-x}$Zn$_x$)$_5$ with (a) $x = 0.025$, (b) 0.035, (c) 0.05, and (d) 0.07 [47], where ΔB indicates $B - B_0$ with $B_0 = 7$ T, 7.4 T, 9 T, and 10 T, respectively. The insets show the image plots of the correlation coefficient r as a function of scaling parameters α and β, resulting from the least squares fitting of the C_e/T data in the scaling analysis. The positions of the maximum r for providing the appropriate α and β values are given by the arrows.

[Figs. 3(a)–3(d)]. Furthermore, a strength of the $-\ln T$ behavior in C_e/T is the same among all the Zn concentrations including pure CeCoIn$_5$ [26]. Note that the specific heat is an extensive variable reflecting the phenomena concerning the large volume. The features above in C_e/T provide evidence that the QCP is located at B^* or B_{M2} and suggest that the high-field AFM order or correlation causing the $-\ln T$ behavior in C_e/T certainly exists below these critical fields. This conclusion is consistent with the B-T phase diagram obtained from the exponent n in the $M/B \propto -T^n$ curves [Figs. 3(a)–3(d)].

We attempt to derive the scaling feature of the C_e/T data to find the connection between the NFL states in pure and Zn-doped CeCoIn$_5$. The scaling curves of the C_e/T data for $x = 0$ and 0.07 were successfully obtained by assuming a scaling function of $[C_e - C_e(B_0)]/(T\Delta B^\alpha) = f[\ln(\Delta B/T^\beta)]$ with $\Delta B = B - B_0$ [26,47]. Thus, we use the same scaling function and procedure for the present scaling analysis. For each x, B_0 was set to be almost identical to B^* or B_{M2}, and a fourth-order polynomial function was tentatively used for $f[\ln(\Delta B/T^\beta)]$ to execute the curve fitting with least squares. The best scaling result was determined so that the correlation coefficient r of the fittings for the given scaling parameters α and β becomes the maximum [the insets of Figs. 6(a)–6(d)]. We checked that the present scaling analysis for our C_e/T data of pure CeCoIn$_5$ (not shown) yields the α and β values of 0.75(6) and 2.6(4), respectively, for $B_0 = 5$ T, which well reproduces the values reported previously ($\alpha = 0.71$ and $\beta = 2.6$) [26]. As displayed in Figs. 6(a)–6(d), we demonstrate that the C_e/T data for all of the Zn concentrations investigated can also be well scaled by the function above, which covers the NFL and FL features in the B range above B^* and B_{M2}. This similarity in the scaling behavior of C_e/T suggests that the NFL state involves a common nature between pure and Zn-doped CeCoIn$_5$; the quantum critical fluctuations are governed by the order parameter corresponding to the high-field AFM state [47].

To elucidate the connection between quantum critical behavior in pure and Zn-doped CeCoIn$_5$ more clearly, we compare the scaling parameters α, β, and B_0 among the Zn concentrations. As summarized in Fig. 7(a), B_0 is found to be linearly enhanced from 5 T ($x = 0$) to 10 T ($x = 0.07$),

reflecting that the QCP is pushed up along with the development of the high-field AFM order. At the same time, it is found that α decreases monotonically with x, while β is roughly unchanged [Fig. 7(b)]. The reduction of α may be simply attributed to the large variations in B_0 with x, because α concerns ΔB as its exponent and is not included in $f[\ln(\Delta B/T^\beta)]$ [47]. In contrast, the nearly constant values of β with all of the x range indicate that the NFL and FL behavior in C_e/T for pure and Zn-doped CeCoIn$_5$ obey the same variable of $\ln(\Delta B/T^\beta)$ with $\beta \approx 2.7$. This trend naturally leads to the conclusion that the order parameter corresponding to the high-field AFM state is responsible for the quantum critical fluctuations in pure and Zn-doped CeCoIn$_5$ [47]. The order parameter evolves as an actual ordered state with the increasing Zn concentrations, although hidden at $B \approx 5$ T and $T \approx 0$ in pure CeCoIn$_5$. The smooth variations of the scaling parameters with x also support this interpretation.
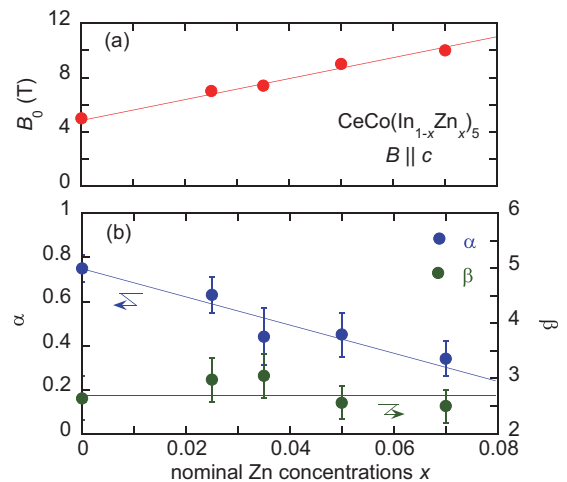

FIG. 7. The scaling parameters (a) B_0, (b) α, and β plotted as a function of the nominal Zn concentrations x for CeCo(In$_{1-x}$Zn$_x$)$_5$ ($x \leqslant 0.07$), which are defined by the formula of $[C_e - C_e(B_0)]/(T\Delta B^\alpha) = f[\ln(\Delta B/T^\beta)]$ with $\Delta B = B - B_0$. The lines are guides for the eye.

IV. DISCUSSION

The present investigation of $CeCo(In_{1-x}Zn_x)_5$ reveals that the critical field of the high-field AFM order continuously decreases with decreasing Zn concentrations along with the shrinkage of the ordered-phase region in the B-T plane and then coincides with the QCP located at $\approx H_{c2}$ in pure $CeCoIn_5$. This result confirms that the quantum critical fluctuations emerging around H_{c2} in $CeCoIn_5$ originate from the "hidden" high-field AFM order parameter, which continuously develops as an actual ordered state with Zn doping [47]. We expect that this finding provides a clue for understanding the unconventional SC properties and quantum critical behavior in $CeCoIn_5$.

First, the high-field AFM order parameter significantly influences the Pauli paramagnetic effect in $CeCoIn_5$, which leads to the emergence of the first-order transition at H_{c2} [6,28] and the possible Fulde-Ferrell-Larkin-Ovchinnikov (FFLO) state just below H_{c2} for $B \| c$ [53]. It is expected that, in the vicinity of H_{c2}, the quantum critical fluctuations originating from the instability of the high-field AFM order markedly enhance spin susceptibility in a wide range of momentum space, including uniform susceptibility as well as staggered susceptibility with the AFM ordering vector. This situation may favor spin-pair breaking of the Cooper pairs rather than the conventional orbital effect when B is applied, yielding the first-order phase transition at H_{c2}. However, once the high-field AFM order occurs with Zn doping, spin susceptibility around H_{c2} is then significantly reduced because the QCP is pushed up to the high-field region away from H_{c2}. For $x \geqslant 0.05$, in addition, the low-field AFM order emerging over the entire SC region also reduces spin susceptibility around H_{c2} [46]. These effects lead to suppression of the Pauli paramagnetic effect. This argument naturally explains the previously observed SC pair-breaking feature in Zn-doped $CeCoIn_5$: The SC pair-breaking mechanism at H_{c2} was found to change from spin-pair breaking to orbital-pair breaking for $B \| c$ as the Zn concentration is increased [46].

In addition, the quantum critical fluctuations of the high-field AFM order may be coupled with the possible FFLO state emerging just below H_{c2} for $B \| c$ [53]. Recent thermal-conductivity measurements under the rotated magnetic field revealed that the possible FFLO phase for $B \| c$ is distinguished from the Q phase observed for $B \perp c$ [54]. It is theoretically suggested that the FFLO and AFM phases become stable in the small region around H_{c2} in the B-T phase diagram when the AFM quantum critical point is located there [24,25]. In this regard, microscopic investigations for the high-field AFM order, such as the AFM structure and Fermi surfaces coupled with AFM ordering, would verify the origin of the possible FFLO state.

Second, the decrease in the Zn concentrations contracts not only the region of the high-field AFM order in the B-T phase diagram but also the anomaly associated with its phase transition in the magnetization and the specific heat. In addition, the anomaly at B_{M2} and T_{M2} in the magnetization and the specific heat is significantly broad even for $x \geqslant 0.05$. These trends reflect the heterogeneous development of the AFM order around the doped Zn ions, similar to the arguments concerning the AFM droplets generated in the Cd-doped $CeCoIn_5$ [43,44,55]. The heterogeneous development of the AFM state is intrinsic and common among the Cd- and Zn-doped $CeCoIn_5$, and such an AFM state is expected to be connected with the quantum critical behavior in $CeCoIn_5$. This trend would be distinguished from the clear AFM order observed around the QCP in the other quantum critical compound $YbRh_2Si_2$ [56]. In Zn-doped $CeCoIn_5$, a reduction in the AFM volume fraction along with the decrease in the Zn ionic concentrations should weaken the anomaly associated with the phase transition in the magnetization and the specific heat, as observed in the present measurements. Recent nuclear magnetic resonance experiments for the high-field AFM phase of Zn-doped $CeCoIn_5$ support this suggestion [48]. In this situation, we expect that a fragment of the high-field AFM order occurs at extremely low temperatures around $\approx H_{c2}$ in $CeCoIn_5$, possibly due to accidental conditions or an intrinsic reason. Such a weak and heterogeneous AFM state would hardly influence usual thermodynamic quantities. Nevertheless, we consider that it could be detected by recent quantum oscillations and nuclear magnetic resonance measurements [31,57].

In accordance with the arguments above, microscopic investigations on the high-field AFM state are necessary to advance exploration of quantum criticality and its relation to the unconventional SC state in $CeCoIn_5$. In particular, it is interesting to clarify the origin of the inhomogeneous AFM state in Zn-doped $CeCoIn_5$ [48], because it can be compared with the AFM droplets induced around the doped ions in the Cd-doped alloys [43,44,55]. Precise measurements of neutron scattering, nuclear magnetic resonance, and muon spin relaxation are being conducted for Zn-doped $CeCoIn_5$.

V. CONCLUSION

Magnetization and specific-heat measurements for $CeCo(In_{1-x}Zn_x)_5$ with $x \leqslant 0.07$ reveal that the high-field AFM order observed for $x = 0.07$ [47] is weakened with decreasing x, accompanied by continuous reduction of its critical field toward ≈ 5 T for $x \to 0$, at which the QCP is realized in $CeCoIn_5$. The T-B-x phase diagram for the Zn-doped alloys was drawn based on those observations. Furthermore, the spatial inhomogeneity of the high-field AFM phase is likely pronounced with decreasing x, yielding the suppression of the anomaly associated with the AFM transition.

At the same time, NFL behavior, characterized by $-\ln T$ dependence in C_e/T, emerges at the critical field for the entire x range below 0.07, followed by recovery of the FL state with further increasing B. Assuming the relation of $[C_e - C_e(B_0)]/(T \Delta B^\alpha) = f[\ln(\Delta B/T^\beta)]$ with $\Delta B = B - B_0$ [26,47], we obtained scaling curves of specific-heat data for the NFL-FL crossover region, and the scaling parameters α, β, and B_0 are continuously connected between pure and Zn-doped $CeCoIn_5$. In particular, the nearly constant values of β between them indicate that the NFL and FL behavior in C_e/T obey the same variable, $\ln(\Delta B/T^\beta)$ with $\beta \approx 2.7$, throughout the development of the high-field AFM order with increasing x. These features provide solid evidence that the order parameter corresponding to the high-field AFM state,

not the other AFM mode such as the low-field AFM order parameter, is responsible for the quantum critical fluctuations in pure and Zn-doped CeCoIn$_5$ [47]. This finding paves the way for further understanding of the origin of unusual SC properties coupled with the quantum criticality in CeCoIn$_5$, such as the first-order transition at H_{c2} and the possible FFLO state just below H_{c2}.

[1] P. A. Lee, N. Nagaosa, and X.-G. Wen, Rev. Mod. Phys. **78**, 17 (2006).

[2] G. R. Stewart, Rev. Mod. Phys. **83**, 1589 (2011).

[3] N. D. Mathur, F. M. Grosche, S. R. Julian, I. R. Walker, D. M. Freye, R. K. W. Haselwimmer, and G. G. Lonzarich, Nature (London) **394**, 39 (1998).

[4] C. Pfleiderer, Rev. Mod. Phys. **81**, 1551 (2009).

[5] C. Petrovic, P. G. Pagliuso, M. F. Hundley, R. Movshovich, J. L. Sarrao, J. D. Thompson, Z. Fisk, and P. Monthoux, J. Phys.: Condens. Matter **13**, L337 (2001).

[6] K. Izawa, H. Yamaguchi, Y. Matsuda, H. Shishido, R. Settai, and Y. Onuki, Phys. Rev. Lett. **87**, 057002 (2001).

[7] K. An, T. Sakakibara, R. Settai, Y. Onuki, M. Hiragi, M. Ichioka, and K. Machida, Phys. Rev. Lett. **104**, 037002 (2010).

[8] W. K. Park, J. L. Sarrao, J. D. Thompson, and L. H. Greene, Phys. Rev. Lett. **100**, 177001 (2008).

[9] C. Stock, C. Broholm, J. Hudis, H. J. Kang, and C. Petrovic, Phys. Rev. Lett. **100**, 087001 (2008).

[10] S. Raymond and G. Lapertot, Phys. Rev. Lett. **115**, 037001 (2015).

[11] Y. Song, J. van Dyke, I. K. Lum, B. D. White, S. Jang, D. Yazici, L. Shu, A. Schneidewind, P. Čermák, Y. Qiu, M. B. Maple, D. K. Morr, and P. Dai, Nat. Commun. **7**, 12774 (2016).

[12] D. G. Mazzone, S. Raymond, J. L. Gavilano, P. Steffens, A. Schneidewind, G. Lapertot, and M. Kenzelmann, Phys. Rev. Lett. **119**, 187002 (2017).

[13] C. Stock, J. A. Rodriguez-Rivera, K. Schmalzl, F. Demmel, D. K. Singh, F. Ronning, J. D. Thompson, and E. D. Bauer, Phys. Rev. Lett. **121**, 037003 (2018).

[14] Y. Song, W. Wang, J. S. Van Dyke, N. Pouse, S. Ran, D. Yazici, A. Schneidewind, P. Čermák, Y. Qiu, M. B. Maple, D. K. Morr, and P. Dai, Commun. Phys. **3**, 98 (2020).

[15] I. Eremin, G. Zwicknagl, P. Thalmeier, and P. Fulde, Phys. Rev. Lett. **101**, 187001 (2008).

[16] A. V. Chubukov and L. P. Gor'kov, Phys. Rev. Lett. **101**, 147004 (2008).

[17] V. P. Michal and V. P. Mineev, Phys. Rev. B **84**, 052508 (2011).

[18] A. Bianchi, R. Movshovich, C. Capan, P. G. Pagliuso, and J. L. Sarrao, Phys. Rev. Lett. **91**, 187004 (2003).

[19] K. Kakuyanagi, M. Saitoh, K. Kumagai, S. Takashima, M. Nohara, H. Takagi, and Y. Matsuda, Phys. Rev. Lett. **94**, 047602 (2005).

[20] B.-L. Young, R. R. Urbano, N. J. Curro, J. D. Thompson, J. L. Sarrao, A. B. Vorontsov, and M. J. Graf, Phys. Rev. Lett. **98**, 036402 (2007).

[21] M. Kenzelmann, Th. Strassle, C. Niedermayer, M. Sigrist, B. Padmanabhan, M. Zolliker, A. D. Bianchi, R. Movshovich, E. D. Bauer, J. L. Sarrao, and J. D. Thompson, Science **321**, 1652 (2008).

[22] A. Aperis, G. Varelogiannis, P. B. Littlewood, and B. D. Simons, J. Phys.: Condens. Matter **20**, 434235 (2008).

[23] D. F. Agterberg, M. Sigrist, and H. Tsunetsugu, Phys. Rev. Lett. **102**, 207004 (2009).

[24] Y. Yanase, J. Phys. Soc. Jpn. **77**, 063705 (2008).

[25] Y. Yanase and M. Sigrist, J. Phys. Soc. Jpn. **78**, 114715 (2009).

[26] A. Bianchi, R. Movshovich, I. Vekhter, P. G. Pagliuso, and J. L. Sarrao, Phys. Rev. Lett. **91**, 257001 (2003).

[27] J. Paglione, M. A. Tanatar, D. G. Hawthorn, E. Boaknin, R. W. Hill, F. Ronning, M. Sutherland, L. Taillefer, C. Petrovic, and P. C. Canfield, Phys. Rev. Lett. **91**, 246405 (2003).

[28] T. Tayama, A. Harita, T. Sakakibara, Y. Haga, H. Shishido, R. Settai, and Y. Onuki, Phys. Rev. B **65**, 180504(R) (2002).

[29] Y. Tokiwa, E. D. Bauer, and P. Gegenwart, Phys. Rev. Lett. **111**, 107003 (2013).

[30] H. Sakai, S. E. Brown, S.-H. Baek, F. Ronning, E. D. Bauer, and J. D. Thompson, Phys. Rev. Lett. **107**, 137001 (2011).

[31] H. Shishido, S. Yamada, K. Sugii, M. Shimozawa, Y. Yanase, and M. Yamashita, Phys. Rev. Lett. **120**, 177201 (2018).

[32] R. Hu, Y. Lee, J. Hudis, V. F. Mitrovic, and C. Petrovic, Phys. Rev. B **77**, 165129 (2008).

[33] S. Raymond, S. M. Ramos, D. Aoki, G. Knebel, V. P. Mineev, and G. Lapertot, J. Phys. Soc. Jpn. **83**, 013707 (2014).

[34] D. G. Mazzone, S. Raymond, J. L. Gavilano, E. Ressouche, C. Niedermayer, J. O. Birk, B. Ouladdiaf, G. Bastien, G. Knebel, D. Aoki, G. Lapertot, and M. Kenzelmann, Sci. Adv. **3**, e1602055 (2017).

[35] D. L. Kunwar, R. B. Adhikari, N. Pouse, M. B. Maple, M. Dzero, and C. C. Almasan, Phys. Rev. B **103**, 224519 (2021).

[36] V. S. Zapf, E. J. Freeman, E. D. Bauer, J. Petricka, C. Sirvent, N. A. Frederick, R. P. Dickey, and M. B. Maple, Phys. Rev. B **65**, 014506 (2001).

[37] M. Yokoyama, H. Amitsuka, K. Matsuda, A. Gawase, N. Oyama, I. Kawasaki, K. Tenya, and H. Yoshizawa, J. Phys. Soc. Jpn. **75**, 103703 (2006).

[38] M. Yokoyama, N. Oyama, H. Amitsuka, S. Oinuma, I. Kawasaki, K. Tenya, M. Matsuura, K. Hirota, and T. J. Sato, Phys. Rev. B **77**, 224501 (2008).

[39] S. Ohira-Kawamura, H. Shishido, A. Yoshida, R. Okazaki, H. Kawano-Furukawa, T. Shibauchi, H. Harima, and Y. Matsuda, Phys. Rev. B **76**, 132507 (2007).

[40] S. K. Goh, J. Paglione, M. Sutherland, E. C. T. O'Farrell, C. Bergemann, T. A. Sayles, and M. B. Maple, Phys. Rev. Lett. **101**, 056402 (2008).

[41] L. D. Pham, T. Park, S. Maquilon, J. D. Thompson, and Z. Fisk, Phys. Rev. Lett. **97**, 056404 (2006).

[42] M. Nicklas, O. Stockert, T. Park, K. Habicht, K. Kiefer, L. D. Pham, J. D. Thompson, Z. Fisk, and F. Steglich, Phys. Rev. B **76**, 052401 (2007).

[43] R. R. Urbano, B.-L. Young, N. J. Curro, J. D. Thompson, L. D. Pham, and Z. Fisk, Phys. Rev. Lett. **99**, 146402 (2007).

[44] S. Seo, X. Lu, J.-X. Zhu, R. R. Urbano, N. Curro, E. D. Bauer, V. A. Sidorov, L. D. Pham, T. Park, Z. Fisk, and J. D. Thompson, Nat. Phys. **10**, 120 (2014).

[45] M. Yokoyama, K. Fujimura, S. Ishikawa, M. Kimura, T. Hasegawa, I. Kawasaki, K. Tenya, Y. Kono, and T. Sakakibara, J. Phys. Soc. Jpn. **83**, 033706 (2014).

[46] M. Yokoyama, H. Mashiko, R. Otaka, Y. Sakon, K. Fujimura, K. Tenya, A. Kondo, K. Kindo, Y. Ikeda, H. Yoshizawa, Y. Shimizu, Y. Kono, and T. Sakakibara, Phys. Rev. B **92**, 184509 (2015).

[47] M. Yokoyama, H. Mashiko, R. Otaka, Y. Oshima, K. Suzuki, K. Tenya, Y. Shimizu, A. Nakamura, D. Aoki, A. Kondo, K. Kindo, S. Nakamura, and T. Sakakibara, Phys. Rev. B **95**, 224425 (2017).

[48] H. Sakai, Y. Tokunaga, S. Kambe, J.-X. Zhu, F. Ronning, J. D. Thompson, S. K. Ramakrishna, A. P. Reyes, K. Suzuki, Y. Oshima, and M. Yokoyama, Phys. Rev. B **104**, 085106 (2021).

[49] M. Haze, Y. Torii, R. Peters, S. Kasahara, Y. Kasahara, T. Shibauchi, T. Terashima, and Y. Matsuda, J. Phys. Soc. Jpn. **87**, 034702 (2018).

[50] T. Sakakibara, H. Mitamura, T. Tayama, and H. Amitsuka, Jpn. J. Appl. Phys. **33**, 5067 (1994).

[51] Note that the phase boundary of the low-field AFM phase for $x = 0.05$ is determined only from the magnetization data.

The specific heat for $x = 0.05$ does not show a peak attributed to the low-field AFM transition whereas its precursor appears as a tail for $T > T_N$ (≈ 2 K), because the peak is masked by the large and sharp jump due to the SC transition when the $T_c \approx T_N$ condition is realized [45]. However, the broad peak or weak kink due to the low-field AFM formation is observed in the temperature and field variations in M [45]. In this situation, the critical field B_{M1} and the transition temperature T_N of the low-field AFM phase in Fig. 3(c) may be slightly overestimated.

[52] R. Movshovich, M. Jaime, J. D. Thompson, C. Petrovic, Z. Fisk, P. G. Pagliuso, and J. L. Sarrao, Phys. Rev. Lett. **86**, 5152 (2001).

[53] K. Kumagai, M. Saitoh, T. Oyaizu, Y. Furukawa, S. Takashima, M. Nohara, H. Takagi, and Y. Matsuda, Phys. Rev. Lett. **97**, 227002 (2006).

[54] S.-Z. Lin, D. Y. Kim, E. D. Bauer, F. Ronning, J. D. Thompson, and R. Movshovich, Phys. Rev. Lett. **124**, 217001 (2020).

[55] H. Sakai, F. Ronning, J.-X. Zhu, N. Wakeham, H. Yasuoka, Y. Tokunaga, S. Kambe, E. D. Bauer, and J. D. Thompson, Phys. Rev. B **92**, 121105(R) (2015).

[56] P. Gegenwart, J. Custers, C. Geibel, K. Neumaier, T. Tayama, K. Tenya, O. Trovarelli, and F. Steglich, Phys. Rev. Lett. **89**, 056402 (2002).

[57] M. Yamashita, M. Tashiro, K. Saiki, S. Yamada, M. Akazawa, M. Shimozawa, T. Taniguchi, H. Takeda, M. Takigawa, and H. Shishido, Phys. Rev. B **102**, 165154 (2020).